Finite-size effects in one-dimensional strained semiconductor heterostructures

Liberato De Caro and Leander Tapfer
Centro Nazionale Ricerca e Sviluppo Materiali (PASTIS-CNRSM), Strada Statale 7 Appia km 712, I-72100 Brindisi, Italy

Antonino Giuffrida
Istituto Nuovi Materiali per L′ Electtronica (CNR-IME) c/o Università degli Studi di Lecce, via Arnesano, I-73100 Lecce, Italy
(Received 22 March 1996; revised manuscript received 31 May 1996)

The elastic lattice deformation of strained one-dimensional (1D) semiconductor heterostructures (quantum wires) is investigated theoretically. We consider the case of lattice-mismatched [100]-oriented superlattices made of cubic symmetry materials with a finite lateral dimension along the [011]- or the [001]-crystallographic direction. Due to the small lateral dimension of the quantum wires, an elastic stress relaxation occurs near the free surfaces. The theoretical evaluation of strain fields in these 1D heterostructures is made with a Fourier series treatment and by using the elasticity theory and the condition of zero total stress on the free surfaces. We also investigate the effect of strain on the confinement potentials. In the case of 1D heterostructures made by materials with zinc-blende symmetry, the nonuniform lattice deformations can induce polarization charges due to the piezoelectric effect. Large band-gap and valence-band-splitting energy modulations of several tens of meV can be obtained near the free surfaces, inducing strong variations in the confinement potentials, which could cause red-shifted electron-hole transitions. Our analytical expressions for the *nonuniform* strain and stress fields, piezoelectric fields, and confinement potentials are valid for any zinc-blende heterostructure made of III-V and II-VI semiconductor compounds. Our results clearly demonstrate that, in addition to the 1D confinement that is caused by the reduced geometrical lateral dimension, the elastic strain relaxation and the piezoelectric fields on the free surfaces of the quantum wires must be considered in order to understand and describe correctly the electronic properties of 1D heterostructures. [S0163-1829(96)02736-1]

I. INTRODUCTION

Low-dimensional strained semiconductor heterostructures, such as quantum-well wires (QWW's), have received much attention in recent years due to the wide range of potential technological applications. The introduction of homogeneous strains in a heterostructure produces changes in the lattice parameter and, in most cases, in the crystallographic symmetry of the material. These effects, added to those induced by the low dimensionality, produce significant changes in the electronic band structure and the vibrational modes, giving the possibility of having wide tunable band gaps, suitable for the realization of new technological devices.[1,2] Quantum confinement effects in QWW's, which are laterally confined by air or vacuum, were experimentally observed and investigated.[3–5]

It was experimentally shown also that in QWW's, which are fabricated by etching layered heterostructures, an elastic relaxation of the lattice strain occurs due to the finite lateral size.[6–8] Recently, we have calculated the *average* lattice deformation of arbitrarily oriented QWW semiconductor heterostructures made of materials with cubic crystallographic symmetry, by using Hooke's law and by imposing the coherence condition at the heterointerfaces only along the wire direction.[9,10] The calculated average lattice deformation has been found to be in very good agreement with the experimental data for the average lattice deformation in QWW heterostructures obtained by high-resolution x-ray-diffraction measurements.[6,7,9] However, it should be noted that in these studies the influence of the finite size of the structure on its local lattice deformation has not been considered. A more realistic description of the actual lattice deformation in QWW's should take into account the partial elastic relaxation of compositional stresses near the free surfaces that is caused by the very small lateral dimensions ($<$200 nm) of these structures and leads to nonuniform strain fields. In fact, photoluminescence experiments revealed that strain release, which may occur on the sidewalls of etched QWW's, causes a band-edge modulation for both the conduction and the valence bands.[8] For this reason an accurate knowledge of the strain and stress fields on the sidewalls and within the QWW's is required in order to have a better understanding and a correct interpretation of the electronic properties of etched low-dimensional structures.

In this work we theoretically investigate the stress relaxation in one-dimensional (1D) strained semiconductor superlattices and calculate the actual lattice deformation field in the whole superlattice volume, even near the free surfaces (sidewalls). Moreover, we analyze the changes in the electronic structures induced by the elastic stress relaxation in 1D heterostructures, due to the finite lateral size. In particular, we evaluate the effect of the nonuniform strain fields on the electron and hole confinement potentials. In fact, in zinc-blende semiconductor materials the obtained lattice deformations could induce internal electric fields via the piezoelectric effect.[11,12]

We consider the case of lattice-mismatched [100]-oriented semiconductor heterostructures made of materials with cubic crystallographic symmetry, with a finite lateral dimension along the [011]- or the [001]-crystallographic direction. The theoretical evaluation of strain fields in the case of 1D heterostructures with a finite lateral dimension along

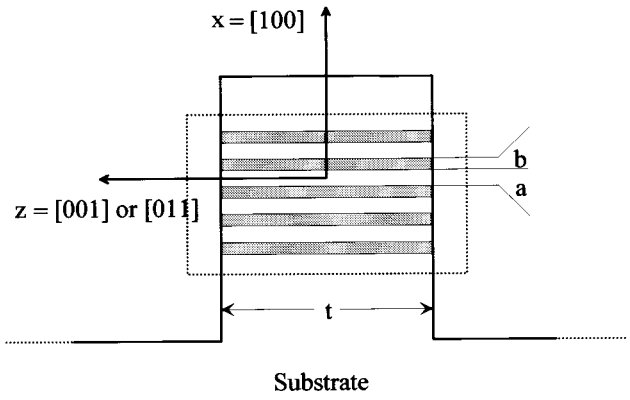

FIG. 1. Schematic diagram of a 1D heterostructure with a finite lateral extension t, made of a two-layer multiple-quantum-well structure. The thickness of the two layers are a and b; the period of the structure is given by $T=a+b$. The dashed rectangle indicates the region of the QWW, where our theoretical model can be applied.

the [001]-crystallographic direction has been made by using a Fourier-series elasticity treatment[13–16] and by imposing the relaxation at the free surfaces of the stresses, induced by the different lattice parameter of the materials constituting the heterostructures. In Refs. 13–16 the theoretical results are applied to the calculations of the strain fields in thinned transmission electron microscopy specimens of lattice-mismatched heterostructures. In this work we extend the theoretical calculations reported in Refs. 13–15 even to the case of a finite size along the [011]-crystallographic direction and apply the obtained results for evaluating the lattice deformations in strained QWW structures.

Our results show that (i) the local lattice spacings of 1D heterostructures is representative of neither the 2D tetragonally distorted material nor the unstressed material; (ii) the obtained strain fields vary by changing the crystallographic direction of finite lateral confinement from the [001] to the [011] orientation; (iii) the lattice deformations depend strongly on the lateral width of the wires; (iv) for 1D heterostructures made by semiconductor materials of zinc-blende symmetry, with a finite lateral dimension along the [011]-crystallographic direction, the nonuniform lattice deformations induce polarization charges due to the piezoelectric effect, located at the intersection of the heterointerface planes with the free surface planes; and (v) if the lattice mismatch is high enough (about 1–2 %), the variation of the lattice deformation can induce strong lateral modulations of the electron and hole confinement potentials (several tens of meV). All the aforementioned effects have a great influence on the mobility of the free carriers and on the electronic energy levels.

II. STRAIN AND STRESS FIELDS

Let us consider a strained superlattice of period T, made of two cubic semiconductor materials A and B with thicknesses a and b, and lattice parameters d_a and d_b, respectively. The superlattice is grown along the **x** crystallographic direction and has a finite lateral width t along the **z** direction (Fig. 1). For the sake of simplicity, let us assume that along the other orthogonal direction **y** the dimension of the superlattice is of infinite extension. This assumption is reasonable and valid for many real QWW structures since the total thickness and the lateral width t of the superlattice is very small in comparison with the wire length. Here we will calculate the strain and the stress fields of the above-mentioned heterostructure, induced by the difference of lattice parameters of the two constituent materials A and B. In these calculations we take into account the partial elastic relaxation of the compositional stresses on the free surfaces located at $\pm t/2$.

Since the superlattice is a periodic structure along the **x** axis, we can search for solutions to our problem with the same periodicity. In fact, choosing the appropriate origin of the reference system (see Fig. 1), the lattice parameter $d(x)$ and, consequently, the lattice mismatch $\varepsilon(x)$ can be expanded in an even Fourier series

$$\varepsilon(x)=\frac{d(x)-\overline{d}}{\overline{d}}=\sum_{p=1}\varepsilon_p\cos(\alpha_p x), \tag{1}$$

where

$$\overline{d}=\frac{a d_a+b d_b}{T},$$

$$\varepsilon_p=2\frac{d_a-d_b}{p\pi\overline{d}}\sin\left(\frac{p\pi a}{T}\right), \tag{2}$$

$$\alpha_p=\frac{2p\pi}{T}.$$

The cosine lattice-mismatch amplitudes ε_p depend on the relative thickness of the two layers A and B. This finding permit us to consider both situations in which the superlattice is either in a free-standing state ($a\approx b$) or pseudomorphic (coherent) with respect to a thick substrate of lattice parameter d_a ($a\gg b$) or d_b ($a\ll b$).

In particular, we are interested in the cases in which **x**=[100], **y**=[011]/$\sqrt{2}$, and **z**=[011]/$\sqrt{2}$ or **x**=[100], **y**=[010], and **z**=[001]. Stress calculations for strained superlattices with a finite size along the [001] crystallographic direction were made by Treacy and Gibson.[13,15] Here we will extend and generalize their calculations to the case of a finite size along the [011] direction and we will apply the obtained results for studying QWW elastic stress relaxation. First, let us consider the particular case **x**=[100], **y**=[011]/$\sqrt{2}$, and **z**=[011]/$\sqrt{2}$, because many QWW's are fabricated with the lateral geometrical confinement along the [011] direction.[2] In fact, we are dealing with a plane deformation problem due to the assumed ''infinite'' extension of the superlattice along the **y** direction. For this reason, all the stress and strain components are functions of the x and z coordinates only.

By using Hooke's equations with respect to the {**x**=[100], **y**=[011]/$\sqrt{2}$, **z**=[011]/$\sqrt{2}$} reference system[17] and by considering the condition of a plane strain problem, the strain compatibility conditions, and the equations of equilibrium in absence of body forces,[18] we obtain the differential equation

$$m_{011}\frac{\partial^2\sigma_{xx}}{\partial z^2}+\frac{\partial^2\sigma_{zz}}{\partial x^2}-n_{011}\frac{\partial^2\sigma_{xz}}{\partial x\partial z}=0, \tag{3}$$

where the σ_{ij} are the stress tensor components and

$$m_{011}=\frac{1+\alpha-2\nu}{2\alpha(1-\nu)}, \quad n_{011}=\frac{\alpha(1+\nu)+1-3\nu}{1-\nu}. \tag{4}$$

Here $\alpha=(C_{11}-C_{12})/2C_{44}$ is the anisotropy coefficient and $\nu=C_{12}/(C_{11}+C_{12})$ is the Poisson ratio, where the C_{ij} are the elastic stiffness constants assumed to be approximately equal in the two semiconductor materials A and B constituting the heterostructure. It should be noted that the coefficients m_{011} and n_{011} of the differential equation (3) differ with respect to those obtained by Treacy and Gibson for superlattices with finite size along the [001]-crystallographic direction.[13,15] In fact, the case of [001] in-plane oriented QWW's can be obtained by substituting the constant coefficients in Eq. (3) by

$$m_{001}=1, \quad n_{001}=\frac{2(\alpha-\nu)}{1-\nu}. \tag{5}$$

Thus, for a finite size along both the [011]- and the [001]-crystallographic direction the same differential equation holds [Eq. (3)], but with different coefficients.[19] Therefore, from now on we will indicate the coefficients of the differential equation (3) without a subscript, but considering the different values for different crystallographic directions where necessary.

Introducing the stress function χ such that

$$\sigma_{xx}=\frac{\partial^2\chi}{\partial z^2}, \quad \sigma_{zz}=\frac{\partial^2\chi}{\partial x^2}, \quad \sigma_{xz}=-\frac{\partial^2\chi}{\partial_x\partial z}, \tag{6}$$

the differential equation [Eq. (3)], which has to be solved, can be written as

$$\frac{\partial^4\chi}{\partial x^4}+m\,\frac{\partial^4\chi}{\partial z^4}+n\,\frac{\partial^4\chi}{\partial x^2\partial z^2}=0. \tag{7}$$

The symmetry of the problem considered gives us the possibility of searching for factorizable solutions of Eq. (7), such as $\chi(x,z)=F(x)G(z)$ with $F(x)=\cos(\alpha_p x)$ for the pth Fourier component.

In order to consider the compositional contribution to the stress components, it is convenient to use the strain suppression method as reported in Ref. 14. In fact, each Fourier component $\cos(\alpha_p x)$ of the series given by Eq. (1) can be considered as a 1D sinusoidal compositional modulation in the x direction, with amplitude ε_p, of a thin film of lateral width t with free surfaces located at $z=\pm t/2$. Thus the boundary conditions of zero total stress (elastic plus compositional ones) on the free surfaces for the pth Fourier component lead to the following conditions for the elastic stresses:[14]

$$\begin{aligned}&\sigma_{xz}(x,\pm t/2)=0, \quad \forall x\in T,\\ &\sigma_{zz}(x,\pm t/2)=-\frac{C_{11}-C_{12}}{C_{11}}(C_{11}+2C_{12})\varepsilon_p\cos(\alpha_p x),\\ &\qquad\qquad \forall x\in T.\end{aligned} \tag{8}$$

We obtain the stress field in the (x,z) plane by solving Eq. (7) and considering the constraints given by Eqs. (8). The analytical expression of the total stress components are reported in the Appendix. Finally, inserting the analytical expression of the total stress components into Hooke's law[17] and taking into account the condition of a plane deformation problem for the elastic strain along the y axis, i.e., $\varepsilon_{yy}^{\mathrm{el}}=0$, we obtain the total strain tensor components as reported in the Appendix.

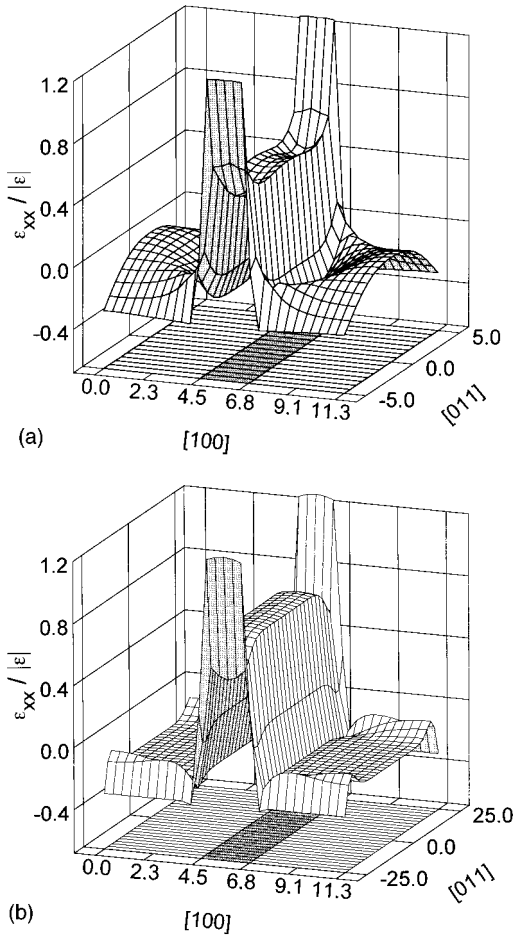

FIG. 2. Total strain ε_{xx}, normalized with respect to the absolute value of the lattice mismatch ε, in one period of a [011]-oriented $GaAs/In_{0.2}Ga_{0.8}As$ QWW with (a) $t=10$ nm and (b) $t=50$ nm. The hatched area (strip) in the reference plane indicates the position and the width of the quantum well with respect to the barrier layers.

As an example, we use our model to analyze an etched $GaAs/In_{0.2}Ga_{0.8}As$ [100]-oriented QWW with sidewalls confined by air or vacuum and a finite lateral extension along the [011]- or the [001]-crystallographic direction as shown in Fig. 1. The dashed area schematically indicates the region of the 1D structure in which our theoretical model can be applied rigorously. In fact, very close to the GaAs substrate crystal the compositional stresses cannot relax completely on the free surfaces due to the presence of a two-dimensional surface structure (substrate).

Figure 2(a) shows the calculated normalized total strain $\varepsilon_{xx}/|\varepsilon|$ (Eqs. (A4) with $\mathbf{x}=[100]$ and $\mathbf{z}=[011]/\sqrt{2}$), normalized with respect to the absolute value of the lattice mismatch ε, in one period for the above-mentioned 1D heterostructures. Here we use the following values for the geometrical parameters of the heterostructure: $a=9$ nm,

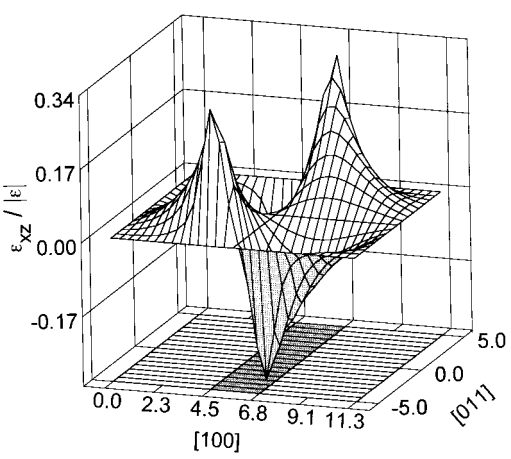

FIG. 3. Elastic shear strain ε_{xz} normalized with respect to the absolute value of the lattice mismatch ε, in one period of a [011]-oriented GaAs/$In_{0.2}Ga_{0.8}As$ QWW with $t=10$ nm.

$b=2.3$ nm, $T=11.3$ nm, and $t=10$ nm. The considered values of the lattice parameters and the stiffness constants for the InAs and GaAs materials are reported in Ref. 20. For the material parameters of the ternary compound the Vegard rule has been used. The differences between the stiffness constants of the two materials constituting the heterostructure were neglected by using averaged values for the whole superlattice period. The Fourier series was truncated at the 40th order in the calculation of the strain components. In fact, in order to obtain a faster convergence of the series, we used the Lanczos averaging method for the calculation of its coefficients.[21] Figure 2(b) shows $\varepsilon_{xx}/|\varepsilon|$ for the same 1D structure of Fig. 2(a), but with increased lateral width $t=50$ nm. A comparison between Figs. 2(a) and 2(b) shows that (i) the lateral size influences the strain fields; (ii) the elastic relaxation strongly modifies the lattice deformation, in particular near the free surfaces; (iii) the elastic relaxation occurs mainly within the 4-nm-thick surface region; and (iv) this last finding implies that for QWW's whose lateral thickness is of the order of 10 nm, the elastic relaxation involves almost the whole volume of the structure. On the other hand, if the QWW thickness is much larger than 10 nm, the elastic relaxation is mainly a surface phenomenon. In fact, in the center $(z=0)$ of the QWW of lateral width $t=50$ nm the total strain field $\varepsilon_{xx}/|\varepsilon|$ approaches the value obtained for a 2D free-standing $In_{0.2}Ga_{0.8}As$ superlattice with the same geometrical parameters T, a, and b. Analogous results can be obtained when the finite size of the QWW is along the [001]-crystallographic direction. However, it is important to note that the strain values averaged along the z direction can change up to 15% as a function of the crystallographic direction, if the t/T ratio becomes very small, i.e., ~ 0.1. In fact, in the limit $t/T \to 0$, the elastic strain limit value of $(1+\nu)\varepsilon$ is approached only if $z=[001]$; on the contrary, if $z=[011]/\sqrt{2}$, the strain limit value of $\{2\alpha(1+\nu)/[\alpha(1+\nu)+1-\nu]\}\varepsilon$ is approached.[9,22]

Figure 3 shows the shear strain component $\varepsilon_{xz}/|\varepsilon|$ [Eqs. (A4)] for the same 1D heterostructures that were considered in Fig. 2(a). It should be noted that, near the intersections of the free surfaces with the heterointerfaces, the shear strain reaches very high values (about $|\varepsilon|/3$). Analogous results can be obtained for the shear strains of QWW's with a finite size along the [001]-crystallographic direction. The low symmetry of the deformed structure has a great influence on its electronic properties, as shown in the following sections.

III. PIEZOELECTRIC FIELDS

If the direction of finite width of the QWW is $\mathbf{z}=[011]/\sqrt{2}$, the nonuniform lattice deformation induces a piezoelectric polarization field that is given by[11,12]

$$P_x(x,z)=e_{14}(x)[\varepsilon_{zz}^{\mathrm{tot}}(x,z)-\varepsilon_{yy}^{\mathrm{tot}}(x)]=e_{14}(x)\varepsilon_{zz}^{\mathrm{el}}(x,z),$$
$$P_z(x,z)=2e_{14}(x)\varepsilon_{xz}^{\mathrm{el}}(x,z), \tag{9}$$

where e_{14} is the piezoelectric constant. It is very important to note that in the case of a [100]-oriented GaAs/$In_{0.2}Ga_{0.8}As$ quantum wire with a finite lateral width along the [001]-crystallographic direction only the piezoelectric field component along the y axis is different from zero. Thus 1D structures with finite lateral extension along the [001] direction may have polarization charges only in the presence of heterointerface and surface roughness.[23]

In the absence of free electric charges (or in the presence of a free charge density much lower than the piezoelectric polarization charge density) the Maxwell electrostatic equations lead to[11,24]

$$\nabla^2 V(x,z)=\frac{\rho(x,z)}{\kappa_0\kappa_r(x)}, \tag{10}$$

where V is the electric potential, κ_0 is the vacuum permettivity, κ_r is the relative dielectric constant, and the charge density is given by[25]

$$\begin{aligned}\rho(x,z)&=-\boldsymbol{\nabla}\cdot\mathbf{P}\\&=-e_{14}\sum_p \frac{2(C_{11}-C_{12})(C_{11}+2C_{12})}{\sqrt{m_{011}}C_{11}[\beta_p\sin(\gamma_p t)+\gamma_p\sinh(\beta_p t)]}\\&\quad\times\alpha_p\varepsilon_p\sin(\alpha_p x)[f_p\cosh(\beta_p z)\cos(\gamma_p z)\\&\quad-g_p\sinh(\beta_p z)\sin(\gamma_p z)].\end{aligned} \tag{11}$$

The coefficients α_p, β_p, and γ_p are defined by Eqs. (2) and (A2), whereas the coefficients f_p and g_p are given by

$$\begin{aligned}f_p&=\left[S_{12}\left(1-\frac{S_{12}+S/2}{S_{11}-S/2}\right)-S_{44}\left(\frac{S_{11}+S_{12}}{2S_{11}-S}\sqrt{m_{011}}-1\right)\right]\beta_p\cosh(\beta_p t/2)\sin(\gamma_p t/2)\\&\quad-\left[S_{12}\left(1-\frac{S_{12}+S/2}{S_{11}-S/2}\right)+S_{44}\left(\frac{S_{11}+S_{12}}{2S_{11}-S}\sqrt{m_{011}}+1\right)\right]\gamma_p\sinh(\beta_p t/2)\cos(\gamma_p t/2),\\g_p&=\left[S_{12}\left(1-\frac{S_{12}+S/2}{S_{11}-S/2}\right)-S_{44}\left(\frac{S_{11}+S_{12}}{2S_{11}-S}\sqrt{m_{011}}-1\right)\right]\beta_p\sinh(\beta_p t/2)\cos(\gamma_p t/2)\\&\quad+\left[S_{12}\left(1-\frac{S_{12}+S/2}{S_{11}-S/2}\right)+S_{44}\left(\frac{S_{11}+S_{12}}{2S_{11}-S}\sqrt{m_{011}}+1\right)\right]\gamma_p\cosh(\beta_p t/2)\sin(\gamma_p t/2).\end{aligned} \tag{12}$$

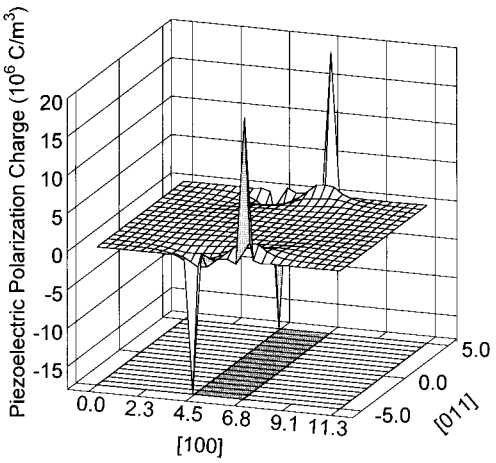

FIG. 4. Polarization charge density in one SL period of a [100]-oriented GaAs/$In_{0.2}Ga_{0.8}As$ QWW with a finite lateral width of $t=10$ nm along the [011]-crystallographic direction.

Here the S_{ij} are the compliance constants and the coefficient m_{011} is given by Eq. (4). The polarization charge density is calculated in Fig. 4 for a [100]-oriented GaAs/$In_{0.2}Ga_{0.8}As$ QWW with a finite lateral width along the [011]-crystallographic direction. Here, for our calculations we used the following geometrical parameters: $a=9$ nm, $b=2.3$ nm, $T=11.3$ nm, and $t=10$ nm. The considered values of the piezoelectric constants for the InAs and GaAs materials are reported in Ref. 20 and the material parameters of the ternary compound are calculated by using Vegard's rule. The hatched area in the reference planes of Fig. 4 gives the position and the width of the $In_{0.2}Ga_{0.8}As$ quantum well with respect to the GaAs barriers. It should be noted that the fixed charges are located at the intersections of the heterointerfaces with the free surfaces. In Fig. 4 only a cross section of the wire (xz plane at a fixed y value) is shown, but the same result holds for any value of the y coordinate. Therefore, the polarization charges have a stringlike distribution along the whole QWW length, in correspondence with the intersection of the heterointerface planes with the free surface planes (sidewalls). In principle, these fixed charges could be screened by mobile charges in the heterostructures. This result would require an excess of mobile charges by 10^{20} e/cm^3, which is a very high value. Therefore, it should be very likely to have 1D fixed electronic charges in a strained QWW, which affect the carrier motion and the electronic energy levels.

We can solve the Poisson equation [Eq. (10)] by expanding the piezoelectric potential in an odd Fourier series.[25] This is possible due to the translational symmetry of the problem along the x axis (periodicity T) by properly choosing the origin of the reference system:

$$V(x,z)=\sum_p c_p(z)\sin(\alpha_p x). \tag{13}$$

Solving the differential equation (10) for the pth Fourier component, we obtain, for electrons,

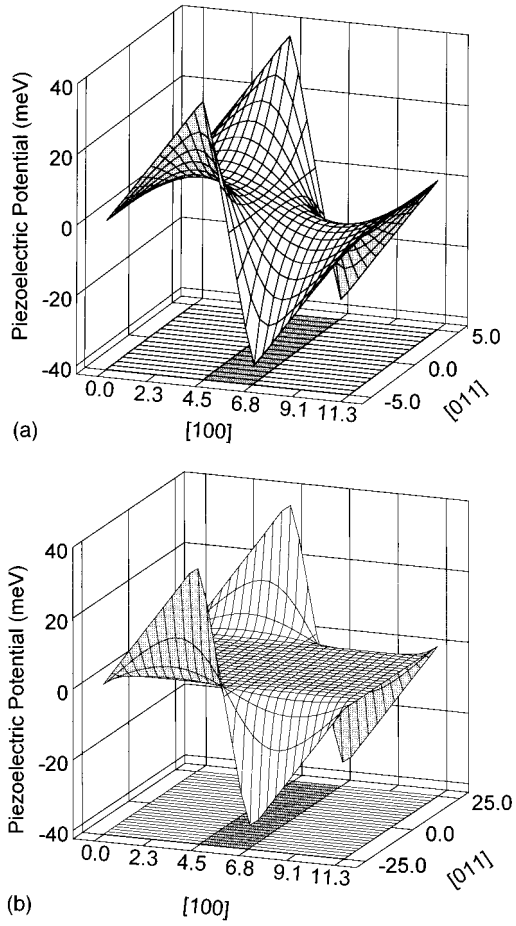

FIG. 5. Piezoelectric potential energy for electrons in meV in one SL period of a [011]-oriented GaAs/$In_{0.2}Ga_{0.8}As$ QWW with (a) $t=10$ nm and (b) $t=50$ nm.

$$\begin{aligned} c_p(z)=&-\frac{e_{14}\varepsilon_p}{2\kappa_0\kappa_r\alpha_p(1+m_{011}-n_{011})}\{[g_p\sqrt{4m_{011}-n_{011}^2} \\ &+f_p(n_{011}-2m_{011})]\cosh(\beta_p z)\sin(\gamma_p z) \\ &+[f_p\sqrt{4m_{011}-n_{011}^2}-g_p(n_{011} \\ &-2m_{011})]\sinh(\beta_p z)\cos(\gamma_p z)\}, \end{aligned} \tag{14}$$

where n_{011} is defined by Eq. (4) and the coefficients f_p and g_p are given by Eqs. (12).

The piezoelectric potential energy is shown in Fig. 5(a) for a [100]-oriented GaAs/$In_{0.2}Ga_{0.8}As$ QWW with a finite lateral extension along the [011]-crystallographic direction with $t=10$ and in Fig. 5(b) for the same structure with $t=50$ nm, respectively. It should be noted that, if the lateral thickness of the QWW is 10 nm, the piezoelectric potential energy is a function different from zero in a rather extended region of the superlattice period, reaching the maximum and minimum values of about ± 40 meV in correspondence with the polarization charges at the intersections of the heterointerfaces with the free surfaces. On the other hand, if $t=50$ nm the piezoelectric effect is localized far away from the center of the structure involving only a 4-nm-thick region on the free surfaces.

IV. CONFINEMENT POTENTIALS

The isotropic or hydrostatic components of the strain field give rise to a change of the volume, without disturbing the crystal symmetry, which causes a variation of the fundamental band gap given by[26]

$$E_g(x,z)=a_{\mathrm{DP}}[\varepsilon_{xx}^{\mathrm{tot}}(x,z)+\varepsilon_{yy}^{\mathrm{tot}}(x)+\varepsilon_{zz}^{\mathrm{tot}}(x,z)], \qquad (15)$$

where a_{DP} is the hydrostatic band-gap deformation potential.

Due to the elastic relaxation of compositional stresses near the free surfaces we obtain an anisotropic contribution to the strain field that reduces the cubic symmetry present in the strain-free quantum-well lattice. This removes the degeneracy between light- and heavy-hole bands and leads to a valence-band splitting given by[24]

$$E_s(x,z)=\sqrt{b_{\mathrm{DP}}^2\{[\varepsilon_{xx}^{\mathrm{tot}}(x,z)-\varepsilon_{yy}^{\mathrm{tot}}(x)]^2+\mathrm{c.p.}\}+d_{\mathrm{DP}}^2\{[\varepsilon_{xy}^{\mathrm{el}}(x,z)]^2+\mathrm{c.p.}\}} \qquad (16)$$

where b_{DP} and d_{DP} are the other deformation potentials and c.p. means cyclic permutations on x, y, and z. In the case of a 1D structure with a finite lateral size along the [001]-crystallographic direction the strain components reported in the Appendix can be directly substituted into Eq. (16) in order to obtain the valence-band splitting in the presence of elastic relaxation. On the other hand, if the finite lateral size is along the [011]-crystallographic direction, the strain tensor reported in the Appendix should be rotated since the crystallographic strain components must be used in Eq. (16).

All the strain-induced energy changes $E_g(x,z)$, $E_s(x,z)$, and $eV(x,z)$ added to the heterostructure band offsets contribute to the confinement potentials. For the electron and heavy holes we obtain[24,26]

$$\begin{aligned} E_e(x,z)&=Q_0(E_{\mathrm{QW}}-E_B)+Q_eE_g(x,z)-eV(x,z),\\ -E_{\mathrm{hh}}(x,z)&=(1-Q_0)(E_B-E_{\mathrm{QW}})-(1-Q_e)E_g(x,z)\\ &\quad+E_s(x,z)-eV(x,z). \end{aligned} \qquad (17)$$

Here Q_0 is the offset ratio for the unstrained bands, $Q_e=a_c/a_{\mathrm{DP}}$, where a_c is the hydrostatic deformation potential for the conduction band, and E_{QW} and E_B are the band gaps of the quantum well and the barrier layer, respectively.

Figure 6 shows the modulation of the conduction-band (CB) minimum and the valence-band (VB) maximum (heavy hole) in one superlattice period of the $GaAs/In_{0.2}Ga_{0.8}As$ QWW that is laterally confined along the [001] direction. The wire width is 10 nm. Figure 7 shows the CB minimum and VB maximum for the same QWW with (011) sidewalls. The variation of the CB minimum and VB maximum of the QWW of increased width (50 nm) is shown in Fig. 8. In all the calculations of Figs. 6–8, we considered the GaAs conduction-band minimum of the bulk GaAs as reference in the energy axes. The unstrained energy gap values at 4 K of the materials constituting the heterostructure were taken from Ref. 27, whereas the ratios Q_0 and Q_e were taken from Ref. 28. Figures 6–8 give a 2D representation of the electron and heavy-hole confinement potentials as described by Eqs. (17). The barrier potential on the free surfaces is not shown. It should be noted that in the case of a finite size along the [001]-crystallographic direction the piezoelectric effect is absent, contrary to the lateral confinement along the [011]-crystallographic direction. This finding is evidenced by the slope along the x axis of the confinement potentials in Figs. 7 and 8, which is absent in Fig. 6. However, if $t=50$ nm (Fig. 8) the piezoelectric effect is present only very near the free surfaces (sidewalls), and at the center of the structure the confinement potentials are almost coincident with the values obtainable for a 2D $GaAs/In_{0.2}Ga_{0.8}As$ superlattice with the same thicknesses of the barrier and quantum-well layers. The important feature, which is common for the three cases, is the strong modulation near the free surfaces of the energy band of the quantum well.

In Fig. 9 band-gap modulations in the center of an $In_{0.2}Ga_{0.8}As$ quantum well of a $(100)GaAs/In_{0.2}Ga_{0.8}As$ QWW with a finite lateral extension of 50 nm along the [001]-crystallographic direction (dashed lines) and of a 2D $(100)GaAs/In_{0.2}Ga_{0.8}As$ superlattice (solid lines) are shown, respectively. The interesting result is the conduction- and valence-band bendings near the free surfaces (sidewalls), which should induce quantum confinement effects near the

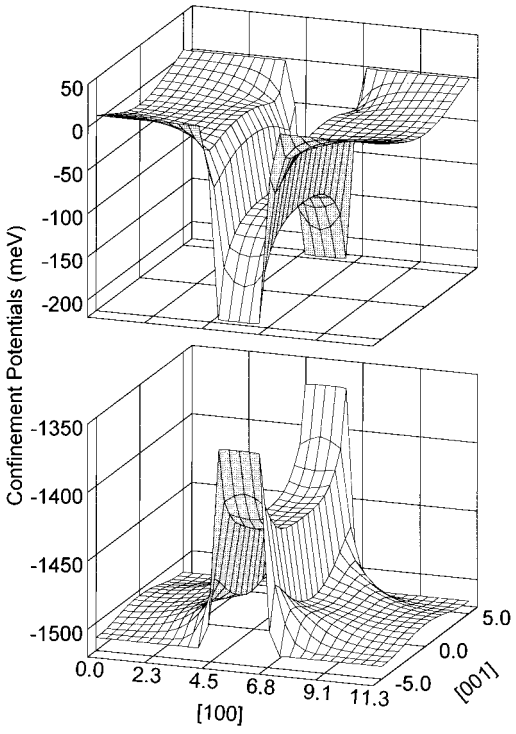

FIG. 6. Electron- and heavy-hole confinement potentials in one SL period of a $GaAs/In_{0.2}Ga_{0.8}As$ [100]-oriented QWW of finite lateral width of 10 nm along the [001]-crystallographic direction. The barrier potential on the free surfaces (sidewalls) is not shown.

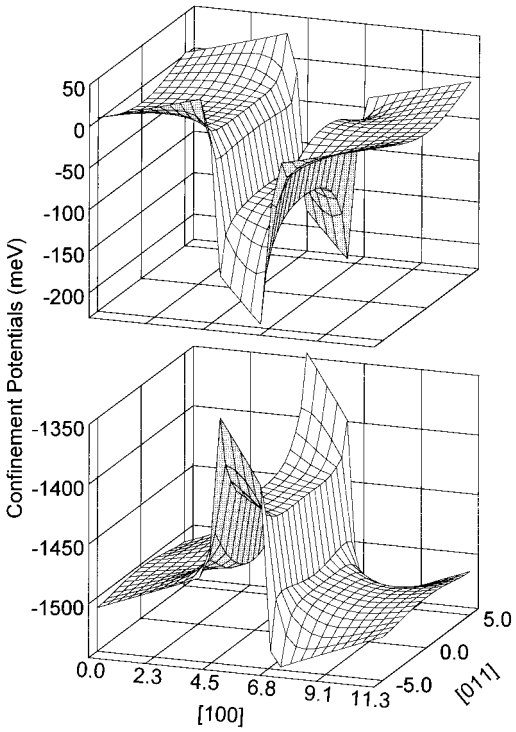

FIG. 7. Electron- and heavy-hole confinement potentials in one SL period of a GaAs/$In_{0.2}Ga_{0.8}As$ [100]-oriented QWW of finite lateral width of 10 nm along the [011]-crystallographic direction.

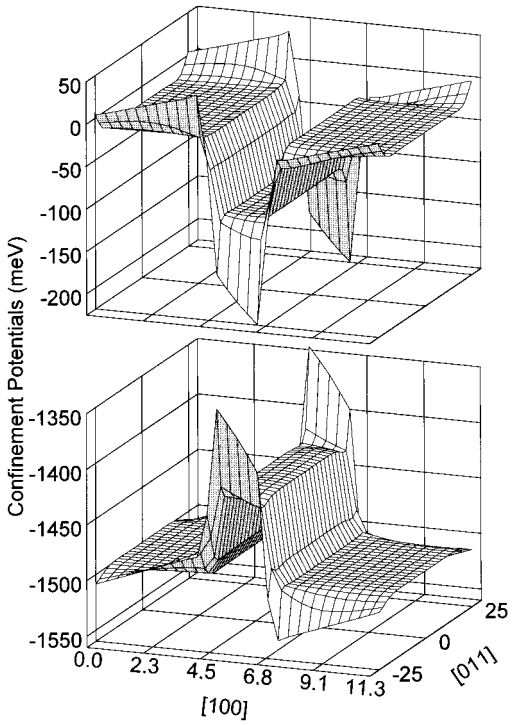

FIG. 8. Electron- and heavy-hole confinement potentials in one SL period of a GaAs/$In_{0.2}Ga_{0.8}As$ [100]-oriented QWW of finite lateral width of 50 nm along the [011]-crystallographic direction.

free surfaces.[29] In fact, the bottom of the squared quantum well 50 nm thick presents almost triangular wells, which are located near the two free surfaces and are about 2.5 nm wide and 90 and 40 meV deep for electrons and heavy holes, respectively. Since these triangular wells are deeper than the CB and VB of the 2D quantum wells and have a width of few nanometers, they should permit the presence of energy levels below the 2D conduction-band minimum for electrons and above the 2D valence-band maximum for the heavy holes, leading to electron-hole transitions that are redshifted with respect to the 2D case. It should be kept in mind that also along the x direction there is a quantum-size effect caused by the finite width b of the $In_{0.2}Ga_{0.8}As$ layer. Thus, even a heterostructure that has a quite large lateral extension (100–200 nm) may give strong quantum-size 1D confinement effects that are generated by the elastic relaxation of the compositional stresses on the free surfaces, but with redshifted excitonic transitions. However, in this case, since the above-mentioned triangular wells are very close to the free surfaces, lateral width fluctuations of the 1D structure should play a crucial role. Moreover, it should be considered that QWW's with a finite lateral size along the [011]-crystallographic direction have polarization charges that are localized in the regions of the triangular wells. Therefore, strong strain-induced electric fields will be generated that may capture the mobile charges on the free surfaces, creating negative effects on the carrier mobility.[30] On the other hand, quantum wires with a finite lateral size along the [001]-crystallographic direction have no polarization charges but have triangular wells near the free surfaces, which are very similar to those shown in Fig. 9. Let us finally note that in the center of the quantum well ($z=0$) there is a relative maximum of the valence band (Fig. 9). This finding should lead to electron-hole transitions from the central area of the QWW, yielding a higher-energy photoluminescence peak with respect to those obtainable from the areas close to the sidewalls of the 1D structure.[31]

V. CONCLUSION

The theoretical model reported in this work allows us to calculate the strain and stress fields in 1D lattice-mismatch [100]-oriented semiconductor heterostructures with a finite lateral dimension along the [011]- or the [001]-

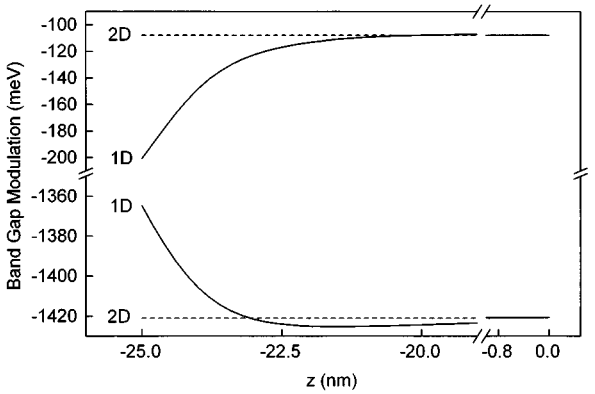

FIG. 9. Band-gap modulation in the center of an $In_{0.2}Ga_{0.8}As$ quantum well of a GaAs/$In_{0.2}Ga_{0.8}As$ [100]-oriented QWW with a finite lateral extension of 50 nm along the [001]-crystallographic direction (solid lines) and, for comparison, of a 2D GaAs/$In_{0.2}Ga_{0.8}As$ [100]-oriented superlattice (dashed lines).

crystallographic direction. The theoretical evaluation of strain fields in these heterostructures has been made with a Fourier series treatment and by using the elasticity theory and the condition of zero total stress on the free surfaces. In particular, we investigated the effects of the elastic relaxation of the compositional stresses on the free surfaces. We show that the lattice deformations in 1D heterostructures can be very different with respect to those of the 2D case. Nonuniform strain fields and lattice plane bendings near the free surfaces occur both in the wells and in the barriers, which strongly depend on the lateral QWW width.

Moreover, we theoretically studied the effect of strain on the confinement potentials of 1D lattice-mismatch semiconductor heterostructures made by materials of zinc-blende crystallographic symmetry. If the QWW's are laterally confined along the [011] direction the nonuniform lattice deformations induce polarization charges due to the piezoelectric effect. These polarization charges are located at the intersection of the heterointerface planes with the free surface planes. These strings of fixed charges can have a strong influence on the electronic properties of 1D heterostructures. No polarization charges are induced in 1D structures with a finite size along the [001]-crystallographic direction.

Due to the elastic relaxation strong lateral modulations in the 1D confinement potentials are obtained. In fact, the bottom of the squared quantum well for electrons of 1D strained structures and the top for holes exhibit almost triangular wells that are located near the two free surfaces. As example we have shown that for (100)GaAs/$In_{0.2}Ga_{0.8}As$ QWW's these triangular wells are several tens of meV deep and can have a width of a few nanometers. Therefore, they could permit the presence of energy levels below the 2D conduction-band minimum for electrons and above the 2D valence-band maximum for the heavy holes, leading to electron-hole transitions that are redshifted with respect to the 2D case.

In summary, our results clearly show that the understanding and correct interpretation of the electronic properties of 1D heterostructures requires one to take into account, besides the 1D confinement caused by the reduced geometrical lateral dimension, the elastic strain relaxation and the piezoelectric fields close to the intersections of the heterointerfaces with the free surfaces of 1D heterostructures.

APPENDIX

Solving Eq. (7) by considering the constraints given by Eqs. (8) and adding the compositional contribution,[14] we obtain the total stress components in the (x,z) plane

$$\begin{aligned}\sigma_{zz}(x,z)=&\sum_p \frac{C_{11}-C_{12}}{C_{11}}(C_{11}+2C_{12})\varepsilon_p\cos(\alpha_p x)\\&\times\left\{\frac{2}{\beta_p\sin(\gamma_p t)+\gamma_p\sinh(\beta_p t)}\right.\\&\times\{[\beta_p\cosh(\beta_p t/2)\sin(\gamma_p t/2)\\&+\gamma_p\sinh(\beta_p t/2)\cos(\gamma_p t/2)]\cosh(\beta_p z)\cos(\gamma_p z)\\&-[\beta_p\sinh(\beta_p t/2)\cos(\gamma_p t/2)-\gamma_p\cosh(\beta_p t/2)\\&\left.\times\sin(\gamma_p t/2)]\sinh(\beta_p z)\sin(\gamma_p z)\}-1\right\},\end{aligned}$$

$$\begin{aligned}\sigma_{xx}(x,z)=&-\sum_p \frac{C_{11}-C_{12}}{C_{11}\sqrt{m}}(C_{11}+2C_{12})\varepsilon_p\cos(\alpha_p x)\\&\times\frac{2}{\beta_p\sin(\gamma_p t)+\gamma_p\sinh(\beta_p t)}\\&\times\{[\beta_p\cosh(\beta_p t/2)\sin(\gamma_p t/2)\\&-\gamma_p\sinh(\beta_p t/2)\cos(\gamma_p t/2)]\cosh(\beta_p z)\cos(\gamma_p z)\\&-[\beta_p\sinh(\beta_p t/2)\cos(\gamma_p t/2)\\&+\gamma_p\cosh(\beta_p t/2)\sin(\gamma_p t/2)]\sinh(\beta_p z)\sin(\gamma_p z)\},\end{aligned}\tag{A1}$$

$$\begin{aligned}\sigma_{xz}(x,z)=&\sum_p \frac{2}{\sqrt{m}(\beta_p\sin(\gamma_p t)+\gamma_p\sinh(\beta_p t))}\\&\times\frac{C_{11}-C_{12}}{C_{11}}\\&\times(C_{11}+2C_{12})\alpha_p\varepsilon_p\sin(\alpha_p x)\\&\times\{\cosh(\beta_p t/2)\sin(\gamma_p t/2)\sinh(\beta_p z)\cos(\gamma_p z)\\&-\sinh(\beta_p t/2)\cos(\gamma_p t/2)\cosh(\beta_p z)\sin(\gamma_p z)\},\end{aligned}$$

where β_p and γ_p are given by

$$\beta_p=\frac{\alpha_p\sqrt{2\sqrt{m}+n}}{2\sqrt{m}},\quad \gamma_p=\frac{\alpha_p\sqrt{2\sqrt{m}-n}}{2\sqrt{m}}.\tag{A2}$$

It is worth noting that if the coefficients m and n assume the values reported in Eqs. (4), then Eqs. (A1) and (A2) will give the stress field for the case of a superlattice with a finite size along the [011]-crystallographic direction with $\mathbf{x}=[100]$, $\mathbf{y}=[011]/\sqrt{2}$, and $\mathbf{z}=[011]/\sqrt{2}$. Contrarily, if the coefficients m and n assume the values reported in Eqs. (5), then Eqs. (A1) and (A2) will give the stress field for the case of a superlattice with a finite size along the [001]-crystallographic direction with $\mathbf{x}=[100]$, $\mathbf{y}=[010]$, and $\mathbf{z}=[001]$.

Inserting Eqs. (A1) into the Hooke law,[17] by using the condition $\varepsilon_{yy}^{\mathrm{el}}=0$, and remembering that the elastic and total strain tensor components are related as

$$\varepsilon_{ij}^{\mathrm{tot}}(x,z)=\varepsilon_{ij}^{\mathrm{el}}-\sum_p \varepsilon_p\cos(\alpha_p x)\,\delta_{ij},\tag{A3}$$

where δ_{ij} is the Kronecker delta tensor, we can obtain the total strain tensor components

$$\begin{aligned}\varepsilon_{xx}^{\mathrm{tot}}(x,z)=&\sum_p \varepsilon_p\cos(\alpha_p x)\left\{\frac{C_{11}-C_{12}}{C_{11}\sqrt{m}}(C_{11}+2C_{12})\right.\\&\times\left[\frac{2}{\beta_p\sin(\gamma_p t)+\gamma_p\sinh(\beta_p t)}\right.\\&\times[r_p\cosh(\beta_p z)\cos(\gamma_p z)\\&+s_p\sinh(\beta_p z)\sin(\gamma_p z)]\\&\left.\left.-S_{12}\left(1-\frac{S_{12}+S/2}{S_{11}-S/2}\right)\sqrt{m}\right]-\frac{S_{12}}{S_{11}-S/2}\right\},\end{aligned}$$

$$\varepsilon_{zz}^{\mathrm{tot}}(x,z)=\sum_p \varepsilon_p \cos(\alpha_p x)\left\{\frac{C_{11}-C_{12}}{C_{11}\sqrt{m}}(C_{11}+2C_{12})\right.$$
$$\times\left[\frac{2}{\beta_p \sin(\gamma_p t)+\gamma_p \sinh(\beta_p t)}\right.$$
$$\times[u_p \cosh(\beta_p z)\cos(\gamma_p z)$$
$$+v_p \sinh(\beta_p z)\sin(\gamma_p z)]-\left(S_{11}-S/2\right.$$
$$\left.\left.-\frac{(S_{12}+S/2)^2}{S_{11}-S/2}\right)\sqrt{m}\right]+\left.\frac{S_{12}+S/2}{S_{11}-S/2}\right\},$$
$$\varepsilon_{yy}^{\mathrm{tot}}(x)=-\sum_p \varepsilon_p \cos(\alpha_p x),$$
$$\varepsilon_{xz}^{\mathrm{tot}}(x,z)=\varepsilon_{xz}^{\mathrm{el}}(x,z)=\sigma_{xz}(x,z)/(2C_{44}),$$

(A4)

where

$$r_p=-\left(S_{11}-\frac{S_{12}^2}{S_{11}-S/2}\right)[\beta_p \cosh(\beta_p t/2)\sin(\gamma_p t/2)$$
$$-\gamma_p \sinh(\beta_p t/2)\cos(\gamma_p t/2)]+S_{12}\left(1-\frac{S_{12}+S/2}{S_{11}-S/2}\right)$$
$$\times[\beta_p \cosh(\beta_p t/2)\sin(\gamma_p t/2)$$
$$+\gamma_p \sinh(\beta_p t/2)\cos(\gamma_p t/2)]\sqrt{m},$$
$$s_p=\left(S_{11}-\frac{S_{12}^2}{S_{11}-S/2}\right)[\beta_p \sinh(\beta_p t/2)\cos(\gamma_p t/2)$$
$$+\gamma_p \cosh(\beta_p t/2)\sin(\gamma_p t/2)]-S_{12}\left(1-\frac{S_{12}+S/2}{S_{11}-S/2}\right)$$
$$\times[\beta_p \sinh(\beta_p t/2)\cos(\gamma_p t/2)$$
$$-\gamma_p \cosh(\beta_p t/2)\sin(\gamma_p t/2)]\sqrt{m},$$
$$u_p=-S_{12}\left(1-\frac{S_{12}+S/2}{S_{11}-S/2}\right)[\beta_p \cosh(\beta_p t/2)\sin(\gamma_p t/2)$$
$$-\gamma_p \sinh(\beta_p t/2)\cos(\gamma_p t/2)]+\left(S_{11}-S/2\right.$$
$$\left.-\frac{(S_{12}+S/2)^2}{S_{11}-S/2}\right)[\beta_p \cosh(\beta_p t/2)\sin(\gamma_p t/2)$$
$$+\gamma_p \sinh(\beta_p t/2)\cos(\gamma_p t/2)]\sqrt{m},$$
$$v_p=S_{12}\left(1-\frac{S_{12}+S/2}{S_{11}-S/2}\right)[\beta_p \sinh(\beta_p t/2)\cos(\gamma_p t/2)$$
$$+\gamma_p \cosh(\beta_p t/2)\sin(\gamma_p t/2)]-\left(S_{11}-S/2\right.$$
$$\left.-\frac{(S_{12}+S/2)^2}{S_{11}-S/2}\right)[\beta_p \sinh(\beta_p t/2)\cos(\gamma_p t/2)$$
$$-\gamma_p \cosh(\beta_p t/2)\sin(\gamma_p t/2)]\sqrt{m}.$$

(A5)

Here the S_{ij} are the elastic compliance constants and $S=S_{11}-S_{12}-S_{44}/2$.[17] Equations (A4) and (A5) were obtained in the case of finite size along the [011]-crystallographic direction. Nevertheless, the same equations can yield the strain tensor components even in the case of finite size along the [001]-crystallographic direction by using Eqs. (5) for the value of m and by setting $S=0$ in order to avoid the rotation of the axes, which is required for $\mathbf{z}=[011]/\sqrt{2}$ but not for $\mathbf{z}=[001]$.

[1] See, for example, *Physics of Nanostructures*, edited by J. H. Davis and A. R. Long, Proceedings of the 38th Scottish University Summer School in Physics, St. Andrews, 1991 (IOP, London, 1992); Vol. 38.

[2] *Science and Engineering of One- and Zero-Dimensional Semiconductors, Vol. 214 of NATO Advanced Study Institute, Series B: Physics*, edited by S. P. Beaumont and C. M. Sotomayor Torres (Plenum, New York, 1990).

[3] R. Cingolani, H. Lage, L. Tapfer, H. Kalt, D. Heitmann, and K. Ploog, Phys. Rev. Lett. **67**, 891 (1991).

[4] P. Ils, M. Michel, A. Forchel, I. Gyuro, M. Klenk, and E. Zielinski, Appl. Phys. Lett. **64**, 496 (1994).

[5] M. Illing, G. Bacher, T. Kümmel, A. Forchel, T. G. Andersson, D. Hommel, B. Jobst, and G. Landwehr, Appl. Phys. Lett. **67**, 124 (1995).

[6] L. Tapfer, G. C. La Rocca, H. Lage, O. Brandt, D. Heitmann, and K. Ploog, Appl. Surf. Sci. **60/61**, 517 (1992).

[7] L. Tapfer, G. C. La Rocca, H. Lage, R. Cingolani, P. Grambow, A. Fischer, D. Heitmann, and K. Ploog, Surf. Sci. **267**, 227 (1992).

[8] I.-H. Tan, R. Mirin, T. Yasuda, E. L. Hu, J. Bowers, C. B. Prater, P. K. Hansma, M. Y. He, and A. G. Evans, J. Vac. Sci. Technol. B **10**, 1971 (1992).

[9] L. De Caro and L. Tapfer, Phys. Rev. B **49**, 11 127 (1994).

[10] L. De Caro and L. Tapfer, Phys. Rev. B **51**, 4381 (1995).

[11] D. L. Smith and C. Mailhiot, J. Appl. Phys. **63**, 2717 (1988).

[12] L. De Caro and L. Tapfer, Phys. Rev. B **51**, 4374 (1995).

[13] J. M. Gibson and M. M. J. Treacy, Ultramicroscopy **14**, 345 (1984).

[14] M. M. J. Treacy, J. M. Gibson, and A. Howie, Philos. Mag. A **51**, 389 (1985).

[15] M. M. J. Treacy and J. M. Gibson, J. Vac. Sci. Technol. B **4**, 1458 (1986).

[16] D. D. Perovic, G. C. Weatherly, and D. C. Houghton, J. Vac. Sci. Technol. A **6**, 1333 (1988); Philos. Mag. A **64**, 1 (1991).

[17] J. F. Nye, *Physical Properties of Crystals* (Oxford University

Press, Oxford, 1964), pp. 93–109 and 131–149.
[18] Yu. A. Amendaze, *Theory of Elasticity* (Mir, Moscow, 1979).
[19] For an isotropic medium we have $\alpha=\alpha_{\rm iso}=1$, $m=m_{\rm iso}=1$, and $n=n_{\rm iso}=2$ and Eq. (3) coincides with the Levy differential equation (Ref. 18).
[20] *Numerical Data and Functional Relationships in Science and Technology*, edited by O. Madelung, M. Schulz, and H. Weiss, Landolt-Börnstein, New Series, Group III, Vol. 17, Pt. a (Springer, Heidelberg, 1982).
[21] F. Scheid, *Numerical Analysis* (McGraw-Hill, New York, 1968).
[22] L. De Caro, A. Giuffrida, and L. Tapfer (unpublished).
[23] M. Ilg, A. Heberle, and K. H. Ploog, Solid State Electron. **37**, 739 (1994).
[24] M. Grundmann, O. Stier, and D. Bimberg, Phys. Rev. B **50**, 14 187 (1994).
[25] By using the Gauss theorem and the symmetry of the electric potential and of the polarization components, it is straightforward to verify that the quantities $\nabla V\cdot\nabla\kappa_r$ and $\nabla e_{14}\cdot\mathbf{P}$ do not contribute to the electric field. In the following we will neglect the differences between the piezoelectric and relative dielectric constants of the two materials constituting the heterostructure by using averaged values in the whole QWW superlattice period.
[26] F. H. Pollak, Semicond. Semimet. **32**, 17 (1990).
[27] K. J. Moore, G. Duggan, K. Woodbridge, and C. Roberts, Phys. Rev. B **41**, 1090 (1990).
[28] S. Niki, C. L. Lin, W. S. C. Chang, and H. H. Wieder, Appl. Phys. Lett. **55**, 1339 (1989).
[29] See, for example, W. Mönch, in *Semiconductor Surface and Interfaces*, edited by Gerhard Ertl, Springer Series in Surface Sciences Vol. 26 (Springer-Verlag, Berlin, 1993), pp. 23–29.
[30] H. Sakaki, J. Appl. Phys. **19**, L735 (1980).
[31] I.-H. Tan, R. Mirin, T. Yasuda, E. L. Hu, J. Bowers, C. B. Prater, P. K. Hansma, M. Y. He, and A. G. Evans, J. Vac. Sci. Technol. B **104**, 1971 (1992).